Research Square

Preprints are preliminary reports that have not undergone peer review.
They should not be considered conclusive, used to inform clinical practice,
or referenced by the media as validated information.

Shared and distinct circadian and molecular effects of ADAR2 deficiency and the Gria2 R/R rescue allele

Maria Lebedeva
National Institute of Mental Health
Kamila Weissova
Charles University
Marek Schwarz
Institute of Microbiology of the Czech Academy of Sciences
Viktor Kuchtiak
Institute of Physiology of the Czech Academy of Sciences
Aneta Kubištova
Charles University
Veronika Spisska
Charles University
Eva Filipovska
Charles University
Dominika Pacesova
Charles University
Irena Svobodova
Charles University
Jan Kubovciak
Institute of Molecular Genetics of the Czech Academy of Sciences
Michal Kolar
Institute of Molecular Genetics of the Czech Academy of Sciences
Zdenka Bendova
zdenka.bendova@natur.cuni.cz

Charles University
Aleš Balík
Institute of Physiology of the Czech Academy of Sciences

Article

Keywords: suprachiasmatic nucleus, circadian rhythms, ADAR2, GluA2, RNA editing, RNA sequencing

Posted Date: September 24th, 2026

DOI: https://doi.org/10.21203/rs.3.rs-10876827/v1

License: This work is licensed under a Creative Commons Attribution 4.0 International License.
Read Full License

Additional Declarations: No competing interests reported.

Abstract

ADAR2-mediated adenosine-to-inosine RNA editing of *Gria2* pre-mRNA generates an arginine codon at the Q/R site, producing the GluA2(R) subunit that confers Ca^{2+} impermeability on AMPA receptors. The survival of *Adar2*$^{-/-}$ mice is ensured by the insertion of the *Gria2*$^{R/R}$ allele. Therefore, phenotype associated with ADAR2 deficiency requires distinction from features shared by mice carrying this rescue allele. We compared background wild-type C57BL/6J (Bl6), *Gria2*$^{R/R}$ and *Adar2*$^{-/-}$/*Gria2*$^{R/R}$ mice using locomotor activity recording, light-pulse-induced phase shifting, immunohistochemistry, RNA sequencing of suprachiasmatic nucleus (SCN) at circadian time 5 (CT5) and CT15, and mass spectrometry-based proteomics of frontal-cortex samples at CT15. Free-running period was similar across genotypes, whereas *Gria2*$^{R/R}$ mice displayed reduced locomotor-rhythm amplitude. *Adar2*$^{-/-}$ mice showed a larger phase delay after a CT15 light pulse than *Gria2*$^{R/R}$ mice, accompanied by stronger early SCN pERK1/2 immunoreactivity but comparable c-FOS induction. RNA sequencing of SCN samples identified 18, 50 and 53 CT5–CT15 differentially expressed genes in Bl6, *Gria2*$^{R/R}$ and *Adar2*$^{-/-}$ mice, respectively, with six genes shared across all genotypes. Most genotype-associated transcriptional differences from Bl6 were shared by the two modified lines: 149 phase-persistent differentially expressed genes were common to both contrasts, whereas direct comparison identified only one gene at CT5 and three at CT15. Proteomics analysis of frontal cortex showed a parallel pattern, with 65 shared proteins and 15 direct differences. These findings associate the broad molecular divergence from Bl6 with the genomically encoded *Gria2*$^{R/R}$ allele and/or shared genetic background, while linking ADAR2 deficiency specifically to enhanced acute photic signalling and circadian resetting.

1. Introduction

The suprachiasmatic nucleus (SCN) serves as the major circadian pacemaker in mammals. It generates self-sustained molecular and electrical rhythms and coordinates physiological processes that show daily rhythmicity. The molecular clockwork responsible for endogenous periodicity is based on transcriptional/translational feedback loops involving CLOCK and BMAL1, which form an activating complex, and PERIOD and CRYPTOCHROME proteins, which form repressive complexes. A second regulatory loop involves *Nr1d1*, encoding the nuclear receptor REV-ERBα, and *Rorα*. REV-ERBα represses, whereas RORα promotes, *Bmal1* transcription [1].

Alignment of endogenous circadian oscillations with external time is achieved primarily through daily entrainment by the light-dark cycle. In mammals, retinal signals reach the SCN through the retinohypothalamic tract, which uses glutamatergic transmission. Within the SCN, N-methyl-D-aspartate (NMDA) receptors participate in photic entrainment together with α-amino-3-hydroxy-5-methyl-4-isoxazolepropionic acid (AMPA) receptors [2, 3]. Light exposure during the early subjective night induces phase delays, whereas exposure during the late subjective night induces phase advances [3]. Photic stimulation also induces expression of *Per1, Per2* and *c-fos* and activates the p42/44 mitogen-activated protein kinase pathway, reflected by phosphorylation of ERK1/2 (pERK1/2) [4–6].

Post-transcriptional RNA processing, including alternative splicing and RNA editing, is an important mechanism to diversify and fine-tune the functional properties of newly synthesized proteins. RNA editing can alter coding sequences as well as structural and regulatory regions of RNA transcripts. Adenosine-to-inosine (A/I) RNA editing is catalysed by adenosine deaminases acting on RNA (ADARs), mainly ADAR1 and ADAR2. While ADAR1 has a major role in the regulation of innate immune responses, ADAR2 is particularly important in the nervous system, where it modifies transcripts encoding proteins involved in neuronal excitability and synaptic transmission [7, 8]. The best-characterized ADAR2 target is the Q/R site in *Gria2* mRNA, which encodes the GluA2 subunit of the AMPA receptor. Editing converts a genomically encoded glutamine (Q) codon to arginine (R). In the adult brain, this site is edited almost completely, and the presence of arginine in GluA2 determines the low calcium permeability of GluA2-containing AMPA receptors. Incomplete Q/R editing interferes with efficient maturation of *Gria2* mRNA and permits expression of calcium-permeable AMPA receptors, thereby increasing susceptibility to excitotoxic neuronal damage [9]. Therefore, Q/R *Gria2* editing is essential for normal neuronal development, function, and survival [10, 11].

The postnatal lethality of *Adar2*$^{-/-}$ mice can be rescued by replacing the glutamine codon at the *Gria2* Q/R site (Q607) with an arginine codon, thereby generating the *Adar2*$^{-/-}$/*Gria2*$^{R/R}$ mice [11]. This rescue allele constitutively encodes arginine at the Q/R site and thereby bypasses the essential requirement for ADAR2-dependent Q/R editing. It does not, however, restore ADAR2-dependent editing of other transcripts or at other editing sites within *Gria2*. ADAR2-dependent editing is dynamically regulated: neuronal activity has been shown to modulate ADAR2 activity in primary neuronal cultures and several brain regions [12–14], and we previously demonstrated circadian regulation of GluA2 R/G-site editing in the rat SCN [15].

Previous work identified *Adar2* as a CLOCK-BMAL-regulated gene and showed that ADAR2 deficiency in the liver is associated with altered rhythmic RNA editing and reduced rhythmic mRNA expression [16]. At the behavioural level, *Adar2*$^{-/-}$/*Gria2*$^{R/R}$ mice showed altered light-pulse–induced phase advance of locomotor rhythms compared to *Gria2*$^{R/R}$ mice. Similarly, in cultured SCN slices, PACAP-induced phase advances of bioluminescence rhythms were markedly attenuated in *Adar2*$^{-/-}$/*Gria2*$^{R/R}$ mice [17]. These findings implicate ADAR2 in phase-specific mechanisms of photic resetting, but the molecular context of altered light responsiveness in the SCN remains incompletely understood.

Interpretation of phenotypes in *Adar2*$^{-/-}$ mice requires consideration of the *Gria2*$^{R/R}$ rescue background. *Gria2*$^{R/R}$ mice are commonly used as controls for *Adar2*$^{-/-}$ animals because both lines constitutively encode arginine at the GluA2 Q/R site. However, our recent targeted analysis showed that *Gria2*$^{R/R}$ mice differ from wild-type C57BL/6J mice in the rhythmic expression of selected clock genes and AMPA receptor subunits in several brain regions, whereas the liver was less affected [18]. Thus, comparison with wild-type mice is required to define transcriptional and behavioural features associated with the presence of *Gria2*$^{R/R}$ allele, whereas direct comparison of *Gria2*$^{R/R}$ and *Adar2*$^{-/-}$ mice addresses the additional consequences of ADAR2 deficiency on the shared *Gria2*$^{R/R}$ background.

In the present study, we compared wild-type C57BL/6J mice, *Gria2*$^{R/R}$ mice and *Adar2*$^{-/-}$ mice to examine the effects of permanent GluA2 Q replacement to GluA2(R) form and ADAR2 deficiency in the circadian system. We analysed free-running locomotor rhythmicity and light-induced phase shift. We further assessed early light-induced SCN activation in the two *Gria2*$^{R/R}$-background lines using pERK1/2 and c-FOS immunoreactivity. Finally, we used RNA sequencing to examine genotype-associated gene expression, and CT5 versus CT15 expression differences in SCN-containing tissue collected during the first circadian cycle in constant darkness (DD), with particular attention to genes assigned to circadian rhythm and glutamatergic synapse pathways. To determine whether the gene expression differences identified in the SCN extended to another brain region and molecular (protein) level, we complemented these analyses with mass spectrometry (MS)-based proteomic profiling of the frontal cortex at CT15.

2. Materials and Methods

2.1 Animals

Adar2 $^{-/-}$/*Gria2*$^{R/R}$ (referred to as *Adar2*$^{-/-}$ in the text) and *Adar2*$^{+/+}$/*Gria2*$^{R/R}$ (referred to as *Gria2*$^{R/R}$ in the text) were kindly provided by Prof. M. Jantsch, Medical University of Vienna. The *Adar2*$^{-/-}$ mouse strain was originally generated by injection of targeted embryonic cells, with disruption of exon 4 in the *Adar2* gene, into C57BL/6J blastocysts. Heterozygous *Adar2*$^{+/-}$ mice were then crossed with the *Gria2*$^{R/R}$ mouse strain in which the genomically encoded arginine at the Q/R site ensures the expression of GluA2 subunits [11]. *Adar2*$^{-/-}$ mice show normal appearance and life span, although the loss of ADAR2 activity alters several phenotypic parameters [19, 20]. Wild-type C57BL/6J mice (referred to as Bl6 in the text) were used as a reference strain with the native *Gria2*$^{Q/Q}$ genotype.

Mice of both sexes were kept on a 12/12 h LD cycle at a temperature of 23 ± 2°C for two weeks before the experiment, with food and water available *ad libitum*. The light source used in the study was a customized linear daylight-white LED source (CCT 5630 K, Spectrasol, Czech Republic) with a dominant wavelength at 459 nm, producing photopic illuminance of 30 ± 1 lx measured at cage level. Mice used for RNA sequencing and proteomic analyses were euthanized by rapid cervical dislocation without prior anesthesia, performed by trained personnel, followed immediately by brain dissection and tissue collection. Mice used for immunohistochemical analyses were deeply anesthetized with thiopental (50 mg/kg, i.p.) and subsequently transcardially perfused through the ascending aorta, as described in detail in Online Resource 1. The experiments were approved by the institutional animal welfare committee of the Faculty of Science, Charles University, and by the Animal Welfare Advisory Committee of the Ministry of Education, Youth and Sports of the Czech Republic (Protocol No. MSMT-31592/2019-4). All animal experiments were conducted in accordance with the relevant guidelines and regulations and the Guide for the Care and Use of Laboratory Animals of the National Institutes of Health. All methods are reported in accordance with the ARRIVE guidelines.

2.2 Locomotor activity measurement

The locomotor activity of seven adult male wild-type Bl6 mice, ten adult male *Gria2*$^{R/R}$ mice and ten adult male *Adar2*$^{-/-}$ mice was monitored using infrared motion detectors (Mini-Mitter VitalView data-acquisition system). Animals were released into DD, and locomotor activity was recorded for 10 days before light pulse application. Circadian parameters of locomotor activity rhythm, free-running period and rhythm amplitude were determined using ClockLab analysis (Version 6, Actimetrics, Wilmette, Illinois). On day 11, mice received a 15-min light pulse of photopic illuminance 30 ± 1 lx at CT15. A phase shift was detected from activity onsets using ClockLab analysis. Regression lines were fitted to activity onsets during the 10 days preceding the light pulse and during the 9 days following the manipulation, omitting the first post-pulse day. Phase shifts were calculated as the difference between the two regression lines, with positive values denoting phase advances and negative values denoting phase delays.

Statistical analyses were performed using GraphPad Prism version 11. The free-running period, rhythm amplitude and light-pulse-induced phase shift were analysed separately. Differences between Bl6, *Gria2*$^{R/R}$ and *Adar2*$^{-/-}$ mice were assessed using one-way ANOVA followed by Tukey's multiple comparisons test. $P < 0.05$ was considered statistically significant.

2.3 Immunohistochemistry

Immunohistochemical analysis of pERK1/2 and c-FOS was performed to relate the behavioural findings to early SCN activation. *Gria2*$^{R/R}$ and *Adar2*$^{-/-}$ mice were exposed to a 15-min light pulse at CT15 and sampled at defined intervals after the pulse. Detailed protocols, antibody information, and analytical procedures are provided in **Online Resource 1**.

2.4 RNA-seq and expression data analysis

The experimental design for the RNA-seq and supplementary proteomic analyses is shown in Fig. 1. Five animals per genotype and time point were used in this experiment. SCN-containing punches were obtained under visual control from acute hypothalamic slices approximately 1 mm thick using a needle punch with an internal diameter of approximately 1 mm. Samples were washed with PBS and flash-frozen on dry ice. Total RNA was extracted using the RNeasy Plus Micro Kit (Qiagen), either directly from frozen samples or from the aqueous phase obtained following TRIzol Reagent extraction. The extraction workflow was balanced across genotypes and sampling times. Batch effects associated with the extraction workflow were assessed and corrected using ComBat-seq before differential expression analysis.

Fig. 1 Experimental design for SCN RNA-seq and frontal-cortex proteomic analyses.

Wild-type Bl6, Gria2 $^{R/R}$ *and Adar2*$^{-/-}$ *mice were maintained under a LD12:12 and then released into DD to minimize the contribution of acute light-induced transcriptional responses. During the first circadian cycle in DD, SCN-containing hypothalamic tissue was collected at CT5 and CT15, corresponding to subjective day and subjective night, respectively, and processed for RNA-seq analysis. In parallel, frontal cortex tissue collected at CT15 was processed for mass spectrometry-based proteomic analysis (MS). The scheme also*

illustrates the genotype and RNA-editing status of the three lines, including wild-type GluA2 Q/R editing in Bl6 mice, constitutive GluA2 R/R expression in Gria2$^{R/R}$ mice and loss of ADAR2-dependent RNA editing in Adar2$^{-/-}$ mice maintained on the Gria2$^{R/R}$ rescue background

The quantity and quality of isolated RNA were assessed using a NanoDrop ND-2000 spectrophotometer (NanoDrop Technologies) and an Agilent 2100 Bioanalyzer (Agilent Technologies). RNA integrity numbers (RINs) ranged from 6.5 to 9.8. Mean RIN values were comparable among genotypes: 7.6 for Bl6, 8.0 for *Gria2*$^{R/R}$ and 8.2 for Adar2$^{-/-}$ mice. All five samples per genotype and time point were used for library preparation. Five nanograms of total RNA were used as input material, and libraries were prepared using the SMARTer Stranded Total RNA-Seq Kit v2, Pico Input Mammalian (Takara Bio, USA), according to the manufacturer's instructions. The prepared libraries were sequenced in three high-output runs on the Illumina NextSeq 500 platform using a 76 + 76-bp paired-end configuration.

Sequencing data were processed using the nf-core/rnaseq bioinformatics pipeline version 1.4.2 [21] with the *Mus musculus* reference genome GRCm38 and Ensembl release 98. Gene-level abundances were quantified using Salmon [22]. Genes were retained for downstream analysis if they had at least 50 counts in total and at least five reads per sample in at least four samples. Counts were adjusted for the batch associated with initial TRIzol processing of a subset of samples using ComBat-seq [23]. The adjusted count matrix was analysed using DESeq2 [24], and the "ashr" method was used for $\log_2$ fold-change (LFC) shrinkage [25].

Differential expression was analysed using two types of contrasts. First, CT5-versus-CT15 comparisons were performed separately within each genotype to identify differences in expression between the two circadian time points. Positive LFC values indicated higher expression at CT5 than at CT15. For these within-genotype comparisons, differentially expressed genes (DEGs) were defined by an absolute LFC ≥ 0.5, corresponding to an approximately 1.4-fold difference, and an adjusted p value < 0.05. Second, genotype comparisons were performed separately at CT5 and CT15. These comprised *Gria2*$^{R/R}$ versus Bl6, *Adar2*$^{-/-}$ versus Bl6 and the direct *Adar2*$^{-/-}$ versus *Gria2*$^{R/R}$ comparison. Positive LFC values indicated higher expression in the first-named genotype. For these genotype comparisons, DEGs were defined by an absolute LFC of at least 1 (2-fold difference) and an adjusted p value < 0.05.

Heatmaps were generated using the ComplexHeatmap package [26], and Venn diagrams and tables showing overlapping or unique genes were visualized using the online tools at https://bioinformatics.psb.ugent.be/webtools/Venn/.

2.5 Mass spectrometry-based proteomic analysis

Mass spectrometry-based proteomic analysis was performed as a supplementary analysis on frontal cortex samples collected at CT15 from the same experimental cohort. Protein abundance was quantified using data-independent acquisition (DIA) nanoLC-MS/MS analysis, and differentially abundant proteins were identified after $\log_2$ transformation and permutation-based FDR correction. Detailed sample preparation, acquisition, and data-processing procedures are provided in the **Online Resource 1**.

3. Results

3.1 Circadian locomotor rhythms and early SCN responses to light

We first analysed locomotor activity rhythms in DD and the responses to a 15-min light pulse applied during the early subjective night at CT15 in Bl6, *Gria2*$^{R/R}$ and *Adar2*$^{-/-}$ mice. The free-running period of locomotor activity was close to 24 h in all three groups and did not differ significantly among genotypes (Fig. 2a). Rhythm amplitude differed between groups. *Gria2*$^{R/R}$ mice showed reduced locomotor rhythm amplitude compared with Bl6 mice (p = 0.0177) and *Adar2*$^{-/-}$ mice (p = 0.0373), whereas Bl6 and *Adar2*$^{-/-}$ mice showed similar values (Fig. 2b). The phase delay was significantly larger in *Adar2*$^{-/-}$ mice than in *Gria2*$^{R/R}$ mice (p = 0.0413; Fig. 2c). Representative actograms illustrate the phase shift of activity onset after the light pulse in each genotype (Fig. 2d).

Fig. 2 Circadian locomotor rhythms and light-pulse-induced phase shifts in Bl6, Gria2*$^{R/R}$ *and Adar2*$^{-/-}$ *mice. *The comparison of circadian period (a), amplitude (b) in locomotor activity rhythm between wild type Bl6, Gria2*$^{R/R}$ *and Adar2*$^{-/-}$ *mice and the magnitude of phase delay induced by a 15-min light pulse applied at CT15 (c). The p-values indicate pairwise comparisons from Tukey multiple comparisons test following one-way ANOVA. Data are plotted as mean ± SEM, n = 7-10. (d) Representative actograms in ClockLab format for Bl6, Gria2*$^{R/R}$ *and Adar2*$^{-/-}$ *mice. The time of light-pulse (LP) application is indicated by yellow asterisks. Red and blue lines indicate regression lines fitted to activity onsets before and after the light pulse, respectively*

To examine whether the larger phase delay in *Adar2*$^{-/-}$ mice than in *Gria2*$^{R/R}$ mice was accompanied by altered early activation of photic signalling pathways in the SCN, we analysed light-induced pERK1/2 and c-FOS immunoreactivity in the two genotypes. pERK1/2 immunoreactivity was higher in *Adar2*$^{-/-}$ mice than in *Gria2*$^{R/R}$ mice 15 min after the light pulse, whereas c-FOS immunoreactivity did not differ significantly between the genotypes (**Online Resource 1, Fig. S1**).

3.2 Gene expression differences between CT5 and CT15 in SCN-containing tissue from Bl6, Gria2$^{R/R}$ and Adar2$^{-/-}$ mice.

As reported previously, targeted RT-qPCR analysis of *Per1, Per2, Cry2* and *Nr1d1* showed broadly similar temporal expression profiles in the SCN of *Gria2*$^{R/R}$ and *Adar2*$^{-/-}$ mice, with limited differences in individual rhythm parameters [18]. We therefore used RNA-seq followed by DGE analysis to examine phase-dependent gene expression in SCN-containing tissue beyond the selected core clock genes.

Samples were collected during the first cycle in DD, according to the experimental design shown in Fig. 1, and DGE analysis was performed separately for the CT5 versus CT15 contrast in each genotype. Using a threshold of an absolute LFC of at least 0.5, corresponding to an approximately 1.4-fold difference, and

an adjusted p value ≤ 0.05, we identified 18 differentially expressed genes in Bl6 mice, 50 in *Gria2*$^{R/R}$ mice and 53 in *Adar2*$^{-/-}$ mice (Fig. 3; **Online Resource 2**).

The canonical clock gene *Nr1d1*, highlighted as an internal marker of circadian time, showed higher expression at CT5 than at CT15 and had an adjusted p value ≤ 0.05 in all three genotypes, consistent with the expected difference between subjective day and subjective night. However, its absolute LFC reached the predefined threshold of 0.5 only in Bl6 mice.

Six genes were differentially expressed in all three genotypes: *Banp, Hspa1b, Plin4, Tsc22d3* and *Zbtb40* showed lower expression at CT5 than at CT15, whereas *Fabp7* showed higher expression at CT5. The Venn diagram further showed limited overlap among DEG sets identified separately in the three genotypes. Four genes, *Insig1, Dnajb1, Srsf5* and *Fam205a4*, were shared between *Bl6* and *Gria2*$^{R/R}$ mice; one gene, *Mfsd2a*, between *Bl6* and *Adar2*$^{-/-}$ mice, and three genes, *Gm43980, Gm45177* and *S100a16* between *Gria2*$^{R/R}$ and *Adar2*$^{-/-}$ mice (Fig. 3). Thus, the three genotypes retained a small common CT5 versus CT15 expression signature, whereas most genes meeting the predefined differential-expression criteria were detected in only one genotype.

Fig. 3 Phase-dependent differential gene expression in the SCN of Bl6, Gria2 $^{R/R}$ ***and Adar2*** $^{-/-}$ ***mice.***

Volcano plots show the difference in gene expression at CT5 versus CT15 in the SCN of mice strains. The $\log_2$ *fold-change difference on the x-axis is plotted against* $-\log_{10}$ *adjusted p-value on the y-axis. Vertical dashed lines indicate an absolute* $\log_2$ *fold change of 0.5, corresponding to an approximately 1.4-fold difference, and the horizontal dashed line indicates an adjusted p value of 0.05. Red and blue points indicate genes with higher and lower expression at CT5, respectively, that met both predefined criteria; grey points did not meet both criteria. Green points indicate Nr1d1, highlighted as a canonical clock gene and an internal marker of circadian phase. The Venn diagram shows the overlap between the CT5 and CT15 DEG sets identified in the three genotypes. The adjacent boxes list DEGs shared by all three genotypes or by individual pairs of genotypes*

To complement the threshold-based overlap analysis, we compared CT5-versus-CT15 LFC estimates across all three genotypes for the union of 101 genes that met the differential-expression criteria in at least one genotype (Fig. 4; **Online Resource 3**). Of these genes, 64 showed expression differences in the same direction in all three genotypes, including the six genes that met both predefined criteria in all three genotypes. Among transcripts previously reported to show sinusoidal expression in an independent SCN time-series dataset, *Dnajb1, Kirrel2, Mmp14* and *Srsf5* also showed directionally concordant CT5-versus-CT15 differences across genotypes. All four met both differential-expression criteria in *Gria2*$^{R/R}$ mice, and *Dnajb1* and *Srsf5* also did so in Bl6 mice. In *Adar2*$^{-/-}$ mice, their absolute LFC estimates ranged from 0.30 to 0.34 and therefore remained below the predefined effect-size threshold of 0.5. Similarly, *Nr1d1* expression was higher at CT5 than at CT15 in all three genotypes, with LFC estimates of 0.61, 0.44 and 0.30 in Bl6, *Gria2*$^{R/R}$ and *Adar2*$^{-/-}$ mice, respectively; only the estimate in Bl6 mice reached the predefined effect-size threshold. Thus, comparison of continuous fold-change estimates revealed substantial

concordance in the direction of CT5-versus-CT15 expression differences that was not fully captured by the threshold-based overlap of the DEG sets.

Fig. 4 Gene-wise CT5-versus-CT15 fold-change patterns for phase-dependent SCN differentially expressed genes across genotypes. *The plot shows LFC estimates for the 101 genes that met the predefined differential-expression criteria (LFC ≥ 0.5 and adjusted p value ≤ 0.05) in at least one genotype. Each row represents one gene. Genes are ordered according to the CT5-versus-CT15 log2 fold change in Bl6 mice, and the same order is retained in the Gria2$^{R/R}$ and Adar2$^{-/-}$ panels. Positive and negative values indicate higher and lower expression at CT5 than at CT15, respectively. Red and blue points indicate genes with positive and negative fold changes, respectively, that met both predefined criteria. Grey points indicate genes with an adjusted p value ≤ 0.05 but an absolute log2 fold change < 0.5. Black points indicate genes with an available adjusted p value > 0.05, whereas open circles indicate genes for which the adjusted p value was unavailable. Green points indicate Nr1d1, highlighted as a canonical clock gene and an internal marker of the CT5-versus-CT15 phase difference. Asterisks at the limits of the x-axis indicate log_2 fold-change estimates outside the displayed range; exact values are provided in Supplementary Table S2*

3.3 Genotype-dependent transcriptional differences relative to Bl6 mice

To characterize genotype-dependent transcriptional differences in the SCN, we compared gene expression in *Gria2*$^{R/R}$ and *Adar2*$^{-/-}$ mice with that in Bl6 mice at CT5 and CT15. Both genetically modified lines showed extensive transcriptional differences relative to Bl6 at both time points (Fig. 5a; **Online Resource 4**). In *Gria2*$^{R/R}$ mice, 281 DEGs were identified at CT5 and 215 at CT15, whereas the corresponding numbers in *Adar2*$^{-/-}$ mice were 305 and 213, respectively. Comparison across the two time points showed that 162 DEGs in *Gria2*$^{R/R}$ mice were detected at both CT5 and CT15, with 119 restricted to CT5 and 53 to CT15. In *Adar2*$^{-/-}$ mice, 164 DEGs were detected at both time points, with 141 restricted to CT5 and 49 to CT15 (Fig. 5b).

The transcriptional differences that persisted across CT5 and CT15 were largely shared by the two genetically modified lines. Of the 162 persistent DEGs in *Gria2*$^{R/R}$ mice and the 164 persistent DEGs in *Adar2*$^{-/-}$ mice, 149 were common to both lines, representing 92% and 91% of the respective sets (Fig. 5c). Only 13 persistent DEGs were specific to *Gria2*$^{R/R}$ mice and 15 to *Adar2*$^{-/-}$ mice. Thus, both lines exhibited a broad and predominantly shared transcriptional divergence from Bl6.

Adarb1, highlighted in green in the volcano plots, showed the residual presence in *Adar2*$^{-/-}$ mice consistent with the expected pattern associated with aberrant mRNA expressed from the impaired *Adarb1* allele missing intron 3 and exon 4 [11]. *Adarb1* expression was no altered *Gria2*$^{R/R}$ carrying lines in *Gria2*$^{R/R}$ mice relative to Bl6, whereas it was markedly lower in *Adar2*$^{-/-}$ mice relative to Bl6 at both CT5 (LFC = − 2.29) and CT15 (LFC = − 2.13) (Fig. 5a). Direct comparison between *Adar2*$^{-/-}$ and *Gria2*$^{R/R}$ mice confirmed that loss of ADAR2 protein was accompanied by only a small additional set of steady-

state mRNA differences (Fig. 5b; **Online Resource 1, Fig. S2; Online Resource 4**). At CT5, *Adarb1* expression was downregulated in *Adar2*$^{-/-}$ mice, and without any significantly upregulated genes. At CT15, *Adarb1* and *Sox3* showed lower and *Sh3bgrl2* higher expression in *Adar2*$^{-/-}$ mice. *Adarb1* was the only DEG detected at both time points in the direct comparison. Together, these results indicate that most SCN transcriptional differences from Bl6 were shared by the two lines carrying the *Gria2*$^{R/R}$ allele, whereas ADAR2 deficiency contributed a limited additional set of differences.

Fig. 5 Genotype-dependent differential gene expression in the SCN of Gria2$^{R/R}$ and Adar2$^{-/-}$ mice.

(a) Volcano plots show differential gene expression at CT5 and CT15 in Gria2 $^{R/R}$ and Adar2$^{-/-}$ mice relative to Bl6 mice. The x-axis indicates log_2 fold change, with positive and negative values corresponding to higher and lower expression, respectively, in the genetically modified line relative to Bl6. The y-axis indicates − log_{10} adjusted p value. Red and blue points represent genes with higher and lower expression, respectively, that met the predefined differential-expression criteria LFC ≥ 1 and adjusted p value ≤ 0.05). Grey points represent genes that did not meet both criteria. Dashed lines indicate the fold-change and adjusted p-value thresholds. Green points identify Adarb1 irrespective of its differential-expression classification. Adarb1 remained within the non-DEG range in Gria2$^{R/R}$ versus Bl6 comparisons but was significantly downregulated in Adar2$^{-/-}$ mice relative to Bl6 at both CT5 and CT15.

(b) Venn diagrams show the overlap between DEGs identified at CT5 and CT15 for Gria2 $^{R/R}$ versus Bl6, Adar2$^{-/-}$ versus Bl6 and Adar2$^{-/-}$ versus Gria2R/R. Numbers indicate genes detected exclusively at CT5, at both time points or exclusively at CT15. Overlap was defined by gene identity irrespective of the direction of expression change.

(c) Venn diagram comparing the combination of DEGs detected at both CT5 and CT15 in the Gria2 $^{R/R}$ versus Bl6 and Adar2$^{-/-}$ versus Bl6 contrasts. Of these phase-persistent DEGs, 149 were shared between the two contrasts, whereas 13 and 15 were specific to Gria2$^{R/R}$ and Adar2$^{-/-}$ mice, respectively. Complete gene lists, LFC and adjusted p values are provided in Supplementary Tables 3 and 4

To examine whether a similar relationship between the genotypes was detectable in another brain region and at the protein level, we performed a supplementary proteomic analysis of the frontal cortex collected at CT15 from corresponding animals that had undergone RNA-seq analysis. This analysis identified 110 differentially abundant proteins in the *Gria2*$^{R/R}$ versus Bl6 comparison and 91 in the *Adar2*$^{-/-}$ versus Bl6 comparison, compared with 15 in the direct *Adar2*$^{-/-}$ versus *Gria2*$^{R/R}$ contrast. Sixty-five proteins were shared between the two comparisons with Bl6. In contrast to Bl6 and *Gria2*$^{R/R}$, ADAR2 protein was not detected in the samples from *Adar2*$^{-/-}$. (**Online Resource 1, Fig. S3; Online Resource 5**). An exploratory cross-tissue comparison with the CT15 SCN RNA-seq dataset identified 10 gene–protein pairs represented among both SCN DEGs and frontal-cortex differentially abundant proteins in the *Gria2*$^{R/R}$ versus Bl6 comparison and 11 in the *Adar2*$^{-/-}$ versus Bl6 comparison (**Online Resource 1, Fig. S4**). All pairs showed concordant directions of change at the transcript and protein levels, and nine were

common to both genotype contrasts. The cortical proteomic data therefore showed a pattern parallel to the predominantly shared divergence of the two *Gria2*$^{R/R}$ carrying lines from Bl6 observed in the SCN transcriptome. Because transcript and protein abundance were measured in different brain regions, this cross-dataset comparison provides descriptive cross-regional support for the shared molecular pattern.

3.4 Expression profiles of circadian rhythm and glutamatergic synapse pathway genes

Motivated by the altered behavioural response to the CT15 light pulse, we compared the expression profiles of genes assigned to the KEGG Circadian rhythm (mmu04710) and Glutamatergic synapse (mmu04724) pathways [27]. Mean rlog-transformed expression values for Bl6, *Gria2*$^{R/R}$ and *Adar2*$^{-/-}$ mice at CT5 and CT15 were scaled within each gene and displayed as heatmaps, allowing comparison of relative expression across the six genotype–phase groups (Figs. 6 and 7).

The Circadian rhythm pathway retained a clear CT5–CT15 organisation across genotypes (Fig. 6). *Cry2*, *Nr1d1*, *Fbxl21*, *Bhlhe40* and *Prkaa2* showed higher relative values at CT5 in all three genotypes, whereas *Clock*, *Per3* and *Npas2* showed higher relative values at CT15. *Cry1* followed the CT15-high pattern in Bl6 and *Gria2*$^{R/R}$ mice, whereas *Adar2*$^{-/-}$ mice showed a lower relative value at CT15. Similarly, *Nfil3* was higher at CT15 in Bl6 and *Gria2*$^{R/R}$ mice, while the two phases showed comparable relative values in *Adar2*$^{-/-}$ mice. A prominent feature of the *Adar2*$^{-/-}$ profile was a set of low CT15 values, particularly for *Rora*, *Fbxw11*, *Prkab1*, *Fbxl3*, *Bhlhe41*, *Csnk1e* and *Per1*. Conversely, *Gria2*$^{R/R}$ mice showed the highest CT15 values among the three genotypes for *Prkag2*, *Rorb*, *Per3*, *Npas2* and *Nfil3*. Thus, the overall phase-dependent organisation of the pathway was conserved, with selective genotype-dependent differences in individual clock-related genes.

The Glutamatergic synapse pathway displayed a more heterogeneous pattern across genotypes (Fig. 7). Only a subset of the genes met the predefined DEG criterion in the CT5-versus-CT15 comparisons, while the heatmap provided a descriptive view of broader differences in their relative expression patterns. *Gria2* and *Grin2b* were relatively higher at CT15 than at CT5 in all three genotypes. Several other ionotropic receptor genes distinguished the two modified lines. At CT15, *Grin1* and *Gria3* showed high relative values in *Adar2*$^{-/-}$ mice and low relative values in Gria2$^{R/R}$ mice, while Grin2a remained relatively high in *Adar2*$^{-/-}$ mice at both phases but showed a marked CT15 decrease in *Gria2*$^{R/R}$ mice. Contrasting CT15 patterns between the modified lines were also apparent for the metabotropic receptor genes *Grm1*, *Grm5* and *Grm7* and for several *Adcy* family members. Collectively, the clock pathway retained a broadly shared CT5–CT15 organization, whereas glutamatergic signalling genes displayed more heterogeneous genotype-dependent relative expression patterns.

Fig. 6 Expression profiles of circadian rhythm pathway genes in the SCN.

The heatmap shows mean rlog-transformed expression values for genes assigned to the KEGG Circadian rhythm pathway (mmu04710) in Bl6, Gria2$^{R/R}$ *and Adar2*$^{-/-}$ *mice at CT5 and CT15. Values were scaled within*

each gene to visualise relative expression differences across genotypes and circadian phases. Red indicates higher relative expression and blue indicates lower relative expression

Fig. 7 Expression profiles of glutamatergic synapse pathway genes in the SCN.

The heatmap shows mean rlog-transformed expression values for genes assigned to the KEGG Glutamatergic synapse pathway (mmu04724) in Bl6, Gria2$^{R/R}$ and Adar2$^{-/-}$ mice at CT5 and CT15. Values were scaled within each gene to visualise relative expression differences across genotypes and circadian phases. Red indicates higher relative expression and blue indicates lower relative expression

4. Discussion

ADAR2-mediated RNA editing shapes the functional properties of several receptors and ion channels involved in SCN timekeeping [2, 8]. In this study, we examined how exclusive R expression at GluA2 Q/R-site and ADAR2 deficiency affect circadian behaviour, response to photic stimuli and phase-dependent gene expression in the SCN by comparing wild-type Bl6, *Gria2*$^{R/R}$ and *Adar2*$^{-/-}$ mice. All three genotypes showed similar free-running periods, whereas locomotor rhythm amplitude was selectively reduced in *Gria2*$^{R/R}$ mice. Following a light pulse at CT15, *Adar2*$^{-/-}$ mice showed a larger phase delay than *Gria2*$^{R/R}$ mice and stronger early pERK1/2 activation, while c-FOS induction was similar. CT5–CT15 comparisons identified several differentially expressed genes in all modified lines, with only six genes shared among all three genotypes. Gene-scaled heatmaps showed broadly conserved CT5–CT15 expression patterns among circadian pathway genes, alongside more heterogeneous relative expression patterns among genes involved in glutamatergic signaling fundamental for cell-to-cell circadian synchronization and photic regulation of the rhythm. At each sampled phase, the gene expression in two modified lines differed extensively from that of Bl6 but only minimally from one another. The analysis of the frontal-cortex proteome showed the same overall relationship, with most changes from Bl6 shared by the two modified lines.

The behavioural analysis revealed two genotype-dependent effects. The amplitude of the locomotor activity rhythm was lower in *Gria2*$^{R/R}$ mice than in both Bl6 and *Adar2*$^{-/-}$ mice, whereas *Adar2*$^{-/-}$ mice showed a larger phase delay than *Gria2*$^{R/R}$ mice. A lower amplitude may result from reduced activity during the active phase, increased activity during the rest phase, or a less consolidated distribution of activity. Consistent with our results, *Adar2*$^{-/-}$ mice were previously reported to show a tendency towards higher locomotor activity during the first half of the dark phase than *Gria2*$^{R/R}$ controls [20]. Because *Adar2*$^{-/-}$ mice carry the same genomic Q/R-site substitution but showed an amplitude comparable to Bl6 mice, the effect of exclusive GluA2(R) expression appears to depend on the native presence and activity of ADAR2. Loss of other ADAR2-dependent functions may therefore counteract the reduction in locomotor rhythm amplitude observed in Gria2$^{R/R}$ mice.

Photic resetting of the SCN is mediated by glutamate and PACAP released from retinohypothalamic terminals, with partly distinct intracellular mechanisms underlying phase delays and phase advances

[28]. AMPA receptor activation contributes particularly to phase delays during the early subjective night [2], making GluA2 a plausible target through which ADAR2 could affect the CT15 response. ADAR2-dependent editing at the R/G site in the ligand-binding domain represents one potential difference between the modified lines. We previously showed that GluA2 R/G editing in the rat SCN oscillates around 50% and peaks at CT10 [15]. R/G editing generally accelerates recovery from desensitization, although its functional consequences depend on receptor composition and flip/flop splicing which is at least partially regulated via R/G editing [13, 29, 30]. Its known kinetic effect therefore does not by itself provide a straightforward explanation for the enhanced phase delay observed here or the enhanced phase advance reported previously [17]. Further studies should examine whether ADAR2-mediated RNA editing interacts with other pathways involved in phase resetting, including GABAergic signalling [31], the G protein-coupled receptor Gpr176 [32] or adenosine signalling [33].

The larger phase delay at CT15 complements the enhanced phase advance at CT22 reported by Terajima et al. [17]. Those authors found no genotype difference in the phase delay at CT14 after a 30-min, 300-lx pulse, whereas we detected a difference at CT15 using a 15-min, 30-lx pulse. Because phase-shift magnitude depends nonlinearly on irradiance, duration and circadian phase, the stronger stimulus used by Terajima et al. may have reduced the ability to detect a genotype difference [34, 35]. Together, the two studies suggest that ADAR2 can influence both phase delays and phase advances, and the observed effect may depend on the timing and strength of the light pulse.

The light pulse induced the expected increase in pERK1/2 and c-FOS in both genotypes [5, 36]. The activity of ERK1/2 is required for light-induced phase shifts [5, 6]. In the present study, light-induced pERK1/2 immunoreactivity was higher in *Adar2*$^{-/-}$ than in *Gria2*$^{R/R}$ mice shortly after the pulse, whereas c-FOS induction was similar between the two groups. The genotype difference was therefore already evident at the level of early SCN signalling and may contribute to the larger behavioural phase delay.

The comparison between CT5 and CT15 identified six differentially expressed genes shared by Bl6, *Gria2*$^{R/R}$ and *Adar2*$^{-/-}$ mice. *Banp*, *Hspa1b*, *Plin4*, *Tsc22d3* and *Zbtb40* were expressed at lower levels at CT5 than at CT15, whereas *Fabp7* was expressed at a higher level at CT5. All six genes showed differences in the same direction between CT6 and CT14 in the liver dataset reported by Terajima et al. [16]. Three of them, *Banp*, *Tsc22d3* and *Fabp7*, also showed sinusoidal expression profiles in the SCN transcriptomic dataset of Pembroke et al. [37]. *Banp*, *Tsc22d3* and *Zbtb40* encode proteins involved in transcriptional regulation [38, 39], *Hspa1b* encodes an inducible HSP70-family chaperone, *Plin4* is associated with lipid-droplet formation and lipid storage, and *Fabp7* encodes a fatty-acid-binding protein expressed predominantly in glial cells [40]. The circadian regulation of *Fabp7* is particularly well established, as its transcription is controlled by REV-ERBα [41]. These findings show that the same CT5–CT15 differences in this particular group of genes were retained across all three genotypes.

Seven genes met our preset differential expression criteria specifically in Bl6 mice: *Cables1*, *Gm10184*, *Gm45767*, *Hsd17b7*, *Nr1d1*, *Opalin* and *Pdgfrb*. In both modified lines, the CT5–CT15 fold changes were smaller: the direction was retained for *Cables1 (down-regulated), Hsd17b7*, *Nr1d1*, *Opalin* and *Pdgfrb (up-*

regulated), whereas the differences in *Gm10184* and *Gm45767* were almost absent. This parallel attenuation in *Gria2*$^{R/R}$ and *Adar2*$^{-/-}$ mice suggests an influence of the *Gria2*$^{R/R}$ allele or their shared genetic background irrespective of ADAR2 activity.

A possible connection between the *Gria2*$^{R/R}$ allele and these expression differences lies in the close relationship between neuronal activity and molecular rhythmicity in the SCN. In the wild-type adult brain, almost all *Gria2* transcripts are edited at the Q/R site and therefore encode arginine. The introduced *Gria2*$^{R/R}$ allele encodes directly arginine, abolishes RNA editing at this site, and blocks the emergence of a small population of transcripts encoding unedited GluA2(Q). The two situations may consequently differ in ways that extend beyond the predominant amino acid sequence of the mature receptor. For example, an independently generated mouse line expressing GluA2(R) only showed higher dendritic spine density in hippocampal CA1 than wild-type mice, indicating that genomically encoded expression of GluA2(R) can influence neuronal structure despite the nearly complete editing at the Q/R site being normally present in the adult brain [42]. AMPA-receptor activation can reset the SCN clock, while membrane depolarization, calcium entry, and communication among SCN cells support the amplitude and synchronization of molecular oscillations [2, 43, 44]. A lifelong change in GluA2-dependent synaptic signalling or circuit organisation could therefore contribute to the parallel attenuation of CT5–CT15 differences in both lines carrying the *Gria2*$^{R/R}$ allele. In addition, four genes with previously reported sinusoidal expression in the SCN met the differential-expression criteria in *Gria2*$^{R/R}$ mice. *Dnajb1* and *Kirrel2* were expressed at lower levels at CT5 than at CT15, whereas *Mmp14* and *Srsf5* were expressed at higher levels at CT5. The corresponding differences in *Adar2*$^{-/-}$ mice occurred in the same directions but with considerably smaller fold change. These genes are involved in protein folding, cell adhesion, extracellular-matrix remodeling and alternative splicing, respectively, and therefore do not define a common pathway [45–48]. Their attenuated CT5–CT15 differences may reflect downstream effects of ADAR2 deficiency on RNA processing or neuronal signalling, although none of the four transcripts has been established as a direct ADAR2 target.

The Venn diagram includes only CT5–CT15 comparisons that crossed both the statistical and fold-change thresholds; consequently, some apparently genotype-restricted DEGs arose from quantitative differences around the cut-offs rather than distinct expression patterns. For example, *Mfsd2a* was expressed at a lower level at CT5 in all three genotypes but narrowly missed the fold-change threshold in *Gria2*$^{R/R}$ mice (LFC = − 0.492). By contrast, *Gm43980* and *Gm45177* showed almost identical CT5-low differences in both modified lines and virtually no CT5–CT15 difference in Bl6, more clearly linking their profiles to a property shared by the two lines.

The dominant feature of the transcriptomic comparisons in Fig. 5 is the molecular similarity between the two lines carrying the constitutive *Gria2*$^{R/R}$ allele. Both differed extensively from Bl6, whereas direct comparison of *Adar2*$^{-/-}$ with *Gria2*$^{R/R}$ mice identified only one differentially expressed genes at CT5 and three at CT15, with *Adarb1* as the only difference shared between the two phases. The data, therefore,

separate a broad molecular signature common to the two rescue lines from a much narrower set of expression changes associated specifically with ADAR2 deficiency.

The genomically encoded GluA2(R) form rescues the early lethality caused by ADAR2 deficiency and thereby enables the study of adult *Adar2*$^{-/-}$ mice [11]. This rescue strategy means that both modified lines carrying the *Gria2*$^{R/R}$ allele express only the GluA2(R) form. The extensive molecular signature shared by *Gria2*$^{R/R}$ and *Adar2*$^{-/-}$ mice, therefore, cannot be attributed specifically to ADAR2 deficiency. It may reflect the *Gria2*$^{R/R}$ allele, other features of the shared genetic background, or both.

The cortical proteomic data reproduced the same overall relationship at a subsequent molecular level. Of the proteins differing from Bl6, 65 were shared by the two modified lines and all changed in the same direction, whereas only 15 proteins differed directly between *Adar2*$^{-/-}$ and *Gria2*$^{R/R}$ mice. Thus, the broad similarity of the rescue lines extends from the SCN transcriptome to the frontal cortex proteome, while the direct protein differences suggest selective downstream effects of ADAR2 deficiency on protein abundance in cortical samples. The exploratory cross-tissue comparison showed 10 overlapping SCN transcripts and cortical proteins in *Gria2*$^{R/R}$ mice and 11 in *Adar2*$^{-/-}$ mice, with concordant directions of change in every case and nine molecules shared by both lines. Among these, *Gabra2* encoding alpha 2 subunit of $GABA_A$ receptor provides a possible link to inhibitory signalling and SCN network coordination [49, 50], while the other molecules represent lipid, peroxisomal and mitochondrial metabolism, immune and complement regulation, and extracellular-matrix organization. Their functional diversity suggests that the shared molecular phenotype involves multiple cellular processes rather than one dominant pathway.

The small ADAR2-specific expression signature aligns with ADAR2's primary molecular role in A-to-I editing. Editing modifies coding and non-coding sequences and impacts the RNA processing, thereby altering the properties of the resulting proteins, while total transcript abundance remains largely unchanged [19, 51]. Dillman et al. [19] reported a similar relationship in the frontal cortex of *Adar2*$^{-/-}$/*Gria2*$^{R/R}$ mice: reduced editing was detected at 56 sites, whereas expression and splicing changes were restricted to two genes and three exons. This distinction is particularly relevant in the brain, where several ADAR2 targets encode receptors and ion channels whose functional properties depend on editing [17, 30]. The direct proteomic differences observed here add a selective layer of altered protein abundance, while changes in the sequence, kinetics and activity of edited proteins and their downstream pathways may contribute to functional effects such as the altered pERK response.

The pathway heatmaps provide a complementary view of the SCN transcriptome by examining two gene sets that are directly relevant to the observed phenotype: the molecular circadian clock and the glutamatergic synapse signalling system through which light resets the SCN. The Circadian rhythm pathway (KEGG mmu04710) retained a clear CT5–CT15 organisation in all three genotypes. Several genes, including *Cry2, Nr1d1, Fbxl21, Bhlhe40* and *Prkaa2*, showed relatively higher expression at CT5, whereas *Clock, Cry1, Per3, Npas2* and *Nfil3* showed relatively higher expression at CT15. This broad

preservation of the sampled-phase pattern is consistent with the similar temporal profiles of *Per1, Per2, Cry2* and *Nr1d1* previously detected by RT-qPCR. It is also consistent with the small number of directly differentially expressed genes identified between *Adar2*$^{-/-}$ and *Gria2*$^{R/R}$ mice. Together, these results indicate that the enhanced response to the CT15 light pulse was accompanied by a largely preserved transcriptional organization of the core SCN clock.

Selected clock-related genes nevertheless showed different relative profiles among the genotypes. At CT15, *Adar2*$^{-/-}$ mice displayed lower relative expression of a group that included *Rora*, *Fbxw11*, *Fbxl3*, *Bhlhe41*, *Dbp*, *Csnk1e* and *Per1*. In contrast, *Gria2*$^{R/R}$ mice showed relatively stronger CT15 expression of *Prkag2*, *Rorb*, *Per3*, *Npas2* and *Nfil3*. These differences may reflect small changes in expression level, phase or amplitude; however, the present experimental design cannot distinguish among these possibilities because the two sampling points capture only one contrast within the circadian cycle. Among these clock-related genes, the relative expression patterns of genes encoding SCF ubiquitin-ligase components and AMPK subunits, which regulate CRY stability and link cellular energy state with circadian timing, raise the possibility that differences between the modified lines extend to post-translational clock regulation or metabolic input to the clock [52–54].

The Glutamatergic synapse pathway (KEGG mmu04724) showed a heterogeneous pattern, consistent with its inclusion of diverse receptors, transporters, synaptic scaffold proteins and downstream signalling components. Rather than a uniform increase or decrease across the pathway, individual branches displayed distinct relative profiles across genotype and circadian time. One of the most prominent contrasts occurred at CT15, when a group containing *Grm1, Grm5, Grm7, Grin1, Grin2a, Gria3, Adcy1, Adcy4, Adcy9, Prkacb, Grk3* and *Plcb3* showed relatively higher expression in *Adar2*$^{-/-}$ than in *Gria2*$^{R/R}$ mice. These genes connect glutamate receptors with Ca^{2+} mobilisation, phospholipase C, cAMP-dependent signalling and MAP kinase regulation. A second group, comprising several ionotropic receptor, transporter and postsynaptic scaffold genes, showed prominent differences at CT5. Together, these profiles raise the possibility that the two modified lines differ subtly in the balance among individual branches of glutamatergic signalling.

The glutamatergic synapse pathway also includes genes involved in astrocyte–neuron glutamate–glutamine cycling, including *Glul, Slc1a2, Slc1a3, Slc38a1, Slc38a2* and *Slc38a3*. Astrocytes are active components of the SCN oscillator network, and rhythmic glutamate release from SCN astrocytes can regulate neuronal activity through GluN2C-containing NMDA receptors [55]. Differences in these genes may therefore reflect altered astrocyte–neuron communication as well as changes in neuronal glutamatergic signalling. At the same time, the SCN-containing tissue punches integrate expression across neuronal, astrocytic, oligodendroglial and vascular populations, each with potentially distinct time-dependent expression patterns [56]. This cellular heterogeneity is illustrated by *Opalin*, which is enriched in differentiated oligodendrocytes, *Pdgfrb*, which is strongly expressed in vascular mural cells including pericytes, and *Mfsd2a*, which is characteristic of blood–brain barrier endothelial cells [57–59]. Their expression profiles may therefore reflect regulation within these cell populations, variation in their

representation within the tissue punches, or both. Cell-type-specific expression analyses would help to distinguish these possibilities.

These DEG profiles capture only one layer of glutamatergic regulation. ADAR2-dependent editing has previously been demonstrated in the SCN for transcripts encoding GluA2, GluK2, Cav1.3, Kv1.1, 5-HT2C and $GABA_A$ α3 receptor or channel components [17]. Several of these proteins participate directly or indirectly in the response of SCN neurons to retinal glutamate, and changes in their editing can alter receptor kinetics, ion permeability, channel gating or intracellular signalling while total mRNA abundance remains largely unchanged. Consequently, similar expression levels observed in the heatmap may coexist with different molecular forms and functional properties of the encoded proteins, as illustrated by the ADAR2-dependent *GluA2* R/G variants discussed above.

Taken together, the pathway-specific heatmaps show broadly similar relative expression patterns of the core circadian machinery across the three genotypes, alongside modest genotype- and circadian-time-associated differences in selected clock and glutamatergic signalling components. These differences are compatible with the enhanced light-induced pERK response and larger behavioural phase delay in *Adar2*$^{-/-}$ mice, while the precise transcript-level mechanisms linking ADAR2 deficiency to these phenotypes remain to be determined.

Several limitations define the scope of these findings. The CT5–CT15 RNA-seq comparison identifies phase-dependent expression differences but cannot distinguish changes in circadian phase, amplitude or mean expression, which would require sampling across the full circadian cycle. The present data associate ADAR2 deficiency with enhanced ERK activation and behavioural resetting but do not establish which ADAR2-dependent molecular changes mediate this effect. Finally, the proteomic analysis was performed in the frontal cortex at CT15 and provides evidence that an analogous relationship among the genotypes occurs in another brain region and at the protein level, rather than a direct protein-level validation of the SCN transcriptomic findings.

Overall, most molecular differences from Bl6 were shared by *Gria2*$^{R/R}$ and *Adar2*$^{-/-}$ mice, whereas direct comparison of the two lines revealed only a small number of differences. The shared profile may result from the presence of *Gria2*$^{R/R}$ allele, the common genetic background of the two lines, or both. Thus, differences between *Adar2*$^{-/-}$ and Bl6 mice represent a combination of effects associated with ADAR2 deficiency and features shared by the two modified lines. However, *Adar2*$^{-/-}$ mice showed a stronger light-induced pERK response and a larger behavioural phase delay than *Gria2*$^{R/R}$ mice, indicating a specific effect of ADAR2 deficiency on acute SCN signalling and circadian resetting. The small number of DEGs is consistent with the role of ADAR2 in RNA editing. The relevant edited targets and downstream mechanisms remain to be identified.

Statements and Declarations

Acknowledgments

The *Adar2*$^{-/-}$*/Gria2*$^{R/R}$ mice were generously provided by Prof. M. Jantsch from the Medical University of Vienna. LCMS analyses were performed in Laboratory of Mass Spectrometry at Biocev research center; Faculty of Science, Charles University

Funding

This work was supported by the Czech Science Foundation (grant no. 25-16433S); Charles University Institutional Research Fund (SVV-260790); Grant Agency of Charles University (project no. 277123); Research Project of the Czech Academy of Sciences (RVO: 67985823); and the ELIXIR CZ research infrastructure project (MEYS grant no. LM2023055) including access to computing and storage facilities.

Competing Interests

The authors have no relevant financial or non-financial interests to disclose.

Author Contributions

Aleš Balík and Zdeňka Bendová contributed to the study conception and design. Animal experiments and brain tissue isolation were performed by Maria Lebedeva, Viktor Kuchtiak, Irena Svobodová and Aneta Kubištová. Proteomic analysis was performed by Aleš Balík, Maria Lebedeva and Kamila Weissová. Immunohistochemistry experiments were performed by Veronika Spišská, Eva Filipovská and Dominika Pačesová. RNA-seq, including experimental design and data analysis, was performed by Kamila Weissová, Marek Schwarz, Jan Kubovciak and Michal Kolář. Figures and tables were prepared by Aleš Balík, Marek Schwarz and Zdeňka Bendová. Overall data analysis and the first draft of the manuscript were completed by Aleš Balík and Zdeňka Bendová. All authors commented on previous versions of the manuscript. All authors read and approved the final manuscript.

Data Availability

The datasets generated and/or analysed during the current study are available in the BioStudies repository under ArrayExpress accession number E-MTAB-11408 (https://www.ebi.ac.uk/biostudies/arrayexpress/studies/E-MTAB-11408) and in the ProteomeXchange Consortium via the PRIDE partner repository under dataset identifier PXD083606 (https://www.ebi.ac.uk/pride/archive/projects/PXD083606).

The collection of immunohistochemical images can be found on the Omero server (https://omero.natur.biocev.org/webclient/?show=project-1011).

Ethics approval

The experiments were approved by the institutional animal welfare committee of the Faculty of Science, Charles University, and by the Animal Welfare Advisory Committee of the Ministry of Education, Youth and Sports of the Czech Republic (Protocol No. MSMT-31592/2019-4). All animal experiments were

conducted in accordance with the relevant guidelines and regulations and the Guide for the Care and Use of Laboratory Animals of the National Institutes of Health. All methods are reported in accordance with the ARRIVE guidelines.

Consent to participate

Not applicable.

Consent to publish

Not applicable.

References

1. Maywood, E. S. Synchronization and maintenance of circadian timing in the mammalian clockwork. *Eur. J. Neurosci.* **51**, 229–240. https://doi.org/10.1111/ejn.14279 (2020).
2. Mizoro, Y. et al. Activation of AMPA receptors in the suprachiasmatic nucleus phase-shifts the mouse circadian clock in vivo and in vitro. *PLoS One*. **5**, e10951. https://doi.org/10.1371/journal.pone.0010951 (2010).
3. Golombek, D. A. & Rosenstein, R. E. Physiology of circadian entrainment. *Physiol. Rev.* **90**, 1063–1102. https://doi.org/10.1152/physrev.00009.2009 (2010).
4. Shearman, L. P. et al. Two period homologs: circadian expression and photic regulation in the suprachiasmatic nuclei. *Neuron* **19**, 1261–1269. https://doi.org/10.1016/s0896-6273(00)80417-1 (1997).
5. Butcher, G. Q. et al. The p42/44 mitogen-activated protein kinase pathway couples photic input to circadian clock entrainment. *J. Biol. Chem.* **277**, 29519–29525. https://doi.org/10.1074/jbc.M203301200 (2002).
6. Dziema, H. et al. The ERK/MAP kinase pathway couples light to immediate-early gene expression in the suprachiasmatic nucleus. *Eur. J. Neurosci.* **17**, 1617–1627. https://doi.org/10.1046/j.1460-9568.2003.02592.x (2003).
7. Gallo, A. et al. ADAR RNA editing in human disease; more to it than meets the I. *Hum. Genet.* **136**, 1265–1278. https://doi.org/10.1007/s00439-017-1837-0 (2017).
8. Heraud-Farlow, J. E. & Walkley, C. R. What do editors do? Understanding the physiological functions of A-to-I RNA editing by adenosine deaminase acting on RNAs. *Open. Biol.* **10**, 200085. https://doi.org/10.1098/rsob.200085 (2020).
9. Kawahara, Y. et al. Glutamate receptors: RNA editing and death of motor neurons. *Nature* **427**, 801. https://doi.org/10.1038/427801a (2004).
10. Pellegrini-Giampietro, D. E., Gorter, J. A., Bennett, M. V. & Zukin, R. S. The GluR2 (GluR-B) hypothesis: Ca(2+)-permeable AMPA receptors in neurological disorders. *Trends Neurosci.* **20**, 464–470. https://doi.org/10.1016/s0166-2236(97)01100-4 (1997).

11. Higuchi, M. et al. Point mutation in an AMPA receptor gene rescues lethality in mice deficient in the RNA-editing enzyme ADAR2. *Nature* **406**, 78–81. https://doi.org/10.1038/35017558 (2000).
12. Sanjana, N. E. et al. Activity-dependent A-to-I RNA editing in rat cortical neurons. *Genetics* **192**, 281–287. https://doi.org/10.1534/genetics.112.141200 (2012).
13. Balik, A., Penn, A. C., Nemoda, Z. & Greger, I. H. Activity-regulated RNA editing in select neuronal subfields in hippocampus. *Nucleic Acids Res.* **41**, 1124–1134. https://doi.org/10.1093/nar/gks1045 (2013).
14. Tariq, A. et al. RNA-interacting proteins act as site-specific repressors of ADAR2-mediated RNA editing and fluctuate upon neuronal stimulation. *Nucleic Acids Res.* **41**, 2581–2593. https://doi.org/10.1093/nar/gks1353 (2013).
15. Míková, H. et al. Circadian Regulation of GluA2 mRNA Processing in the Rat Suprachiasmatic Nucleus and Other Brain Structures. *Mol. Neurobiol.* **58**, 439–449. https://doi.org/10.1007/s12035-020-02141-8 (2021).
16. Terajima, H. et al. ADARB1 catalyzes circadian A-to-I editing and regulates RNA rhythm. *Nat. Genet.* **49**, 146–151. https://doi.org/10.1038/ng.3731 (2017).
17. Terajima, H. et al. A-to-I RNA editing enzyme ADAR2 regulates light-induced circadian phase-shift. *Sci. Rep.* **8**, 14848. https://doi.org/10.1038/s41598-018-33114-6 (2018).
18. Lebedeva, M. et al. The disruption of circadian rhythmicity of gene expression in the hippocampus and associated structures in Gria2 mice; a comparison with C57BL/6J and Adar2 mice strains. *Brain Res.* **1826**, 148739. https://doi.org/10.1016/j.brainres.2023.148739 (2024).
19. Dillman, A. A., Cookson, M. R. & Galter, D. ADAR2 affects mRNA coding sequence edits with only modest effects on gene expression or splicing in vivo. *RNA Biol.* **13**, 15–24. https://doi.org/10.1080/15476286.2015.1110675 (2016).
20. Horsch, M. et al. Requirement of the RNA-editing enzyme ADAR2 for normal physiology in mice. *J. Biol. Chem.* **286**, 18614–18622. https://doi.org/10.1074/jbc.M110.200881 (2011).
21. Ewels, P. A. et al. The nf-core framework for community-curated bioinformatics pipelines. *Nat. Biotechnol.* **38**, 276–278. https://doi.org/10.1038/s41587-020-0439-x (2020).
22. Patro, R. et al. Salmon provides fast and bias-aware quantification of transcript expression. *Nat. Methods*. **14**, 417–419. https://doi.org/10.1038/nmeth.4197 (2017).
23. Zhang, Y., Parmigiani, G. & Johnson, W. E. ComBat-seq: batch effect adjustment for RNA-seq count data. *NAR Genom Bioinform*. **2**, lqaa078. https://doi.org/10.1093/nargab/lqaa078 (2020).
24. Love, M. I., Huber, W. & Anders, S. Moderated estimation of fold change and dispersion for RNA-seq data with DESeq2. *Genome Biol.* **15**, 550. https://doi.org/10.1186/s13059-014-0550-8 (2014).
25. Stephens, M. False discovery rates: a new deal. *Biostatistics* **18**, 275–294. https://doi.org/10.1093/biostatistics/kxw041 (2017).
26. Gu, Z., Eils, R. & Schlesner, M. Complex heatmaps reveal patterns and correlations in multidimensional genomic data. *Bioinformatics* **32**, 2847–2849.

https://doi.org/10.1093/bioinformatics/btw313 (2016).

27. Kanehisa, M. & Goto, S. K. E. G. G. Kyoto Encyclopedia of Genes and Genomes. *Nucleic Acids Res.* **28**, 27–30 (2000).
28. Gillette, M. U. & Mitchell, J. W. Signaling in the suprachiasmatic nucleus: selectively responsive and integrative. *Cell. Tissue Res.* **309**, 99–107. https://doi.org/10.1007/s00441-002-0576-1 (2002).
29. Lomeli, H. et al. Control of kinetic properties of AMPA receptor channels by nuclear RNA editing. *Science* **266**, 1709–1713. https://doi.org/10.1126/science.7992055 (1994).
30. Wen, W., Lin, C-Y. & Niu, L. R/G editing in GluA2Rflop modulates the functional difference between GluA1 flip and flop variants in GluA1/2R heteromeric channels. *Sci. Rep.* **7**, 13654. https://doi.org/10.1038/s41598-017-13233-2 (2017).
31. Mintz, E. M. et al. GABA interacts with photic signaling in the suprachiasmatic nucleus to regulate circadian phase shifts. *Neuroscience* **109**, 773–778. https://doi.org/10.1016/s0306-4522(01)00519-x (2002).
32. Yamaguchi, Y. et al. Nmu/Nms/Gpr176 Triple-Deficient Mice Show Enhanced Light-Resetting of Circadian Locomotor Activity. *Biol. Pharm. Bull.* **45**, 1172–1179. https://doi.org/10.1248/bpb.b22-00260 (2022).
33. Jagannath, A. et al. The regulation of circadian entrainment in mice by the adenosine the A 2A /A 1 receptor antagonist CT1500. *Front. Physiol.* **13**, 1085217. https://doi.org/10.3389/fphys.2022.1085217 (2022).
34. Nelson, D. E. & Takahashi, J. S. Sensitivity and integration in a visual pathway for circadian entrainment in the hamster (Mesocricetus auratus). *J. Physiol.* **439**, 115–145. https://doi.org/10.1113/jphysiol.1991.sp018660 (1991).
35. Morin, L. P. & Studholme, K. M. Light pulse duration differentially regulates mouse locomotor suppression and phase shifts. *J. Biol. Rhythms*. **29**, 346–354. https://doi.org/10.1177/0748730414547111 (2014).
36. Illnerová, H. et al. Hormones, subjective night and season of the year. *Physiol. Res.* **49** (Suppl 1), S1–10 (2000).
37. Pembroke, W. G. et al. Temporal transcriptomics suggest that twin-peaking genes reset the clock. *eLife* **4**, e10518. https://doi.org/10.7554/eLife.10518 (2015).
38. Cannarile, L. et al. Cloning, chromosomal assignment and tissue distribution of human GILZ, a glucocorticoid hormone-induced gene. *Cell. Death Differ.* **8**, 201–203. https://doi.org/10.1038/sj.cdd.4400798 (2001).
39. Grand, R. S. et al. BANP opens chromatin and activates CpG-island-regulated genes. *Nature* **596**, 133–137. https://doi.org/10.1038/s41586-021-03689-8 (2021).
40. Chmurzyńska, A. The multigene family of fatty acid-binding proteins (FABPs): function, structure and polymorphism. *J. Appl. Genet.* **47**, 39–48. https://doi.org/10.1007/BF03194597 (2006).

41. Schnell, A. et al. The nuclear receptor REV-ERBα regulates Fabp7 and modulates adult hippocampal neurogenesis. *PLoS One*. **9**, e99883. https://doi.org/10.1371/journal.pone.0099883 (2014).
42. Wright, A. L. et al. The Q/R editing site of AMPA receptor GluA2 subunit acts as an epigenetic switch regulating dendritic spines, neurodegeneration and cognitive deficits in Alzheimer's disease. *Mol. Neurodegener*. **18**, 65. https://doi.org/10.1186/s13024-023-00632-5 (2023).
43. Lundkvist, G. B. et al. A calcium flux is required for circadian rhythm generation in mammalian pacemaker neurons. *J. Neurosci.* **25**, 7682–7686. https://doi.org/10.1523/JNEUROSCI.2211-05.2005 (2005).
44. Yamaguchi, S. et al. Synchronization of cellular clocks in the suprachiasmatic nucleus. *Science* **302**, 1408–1412. https://doi.org/10.1126/science.1089287 (2003).
45. Panda, S. et al. Coordinated transcription of key pathways in the mouse by the circadian clock. *Cell* **109**, 307–320. https://doi.org/10.1016/s0092-8674(02)00722-5 (2002).
46. Yeung, C-Y-C. et al. Mmp14 is required for matrisome homeostasis and circadian rhythm in fibroblasts. *Matrix Biol.* **124**, 8–22. https://doi.org/10.1016/j.matbio.2023.10.002 (2023).
47. McGlincy, N. J. et al. Regulation of alternative splicing by the circadian clock and food related cues. *Genome Biol.* **13**, R54. https://doi.org/10.1186/gb-2012-13-6-r54 (2012).
48. Serizawa, S. et al. A neuronal identity code for the odorant receptor-specific and activity-dependent axon sorting. *Cell* **127**, 1057–1069. https://doi.org/10.1016/j.cell.2006.10.031 (2006).
49. O'Hara, B. F. et al. GABAA, GABAC, and NMDA receptor subunit expression in the suprachiasmatic nucleus and other brain regions. *Brain Res. Mol. Brain Res.* **28**, 239–250. https://doi.org/10.1016/0169-328x(94)00212-w (1995).
50. Freeman, G. M. et al. GABA networks destabilize genetic oscillations in the circadian pacemaker. *Neuron* **78**, 799–806. https://doi.org/10.1016/j.neuron.2013.04.003 (2013).
51. Rueter, S. M., Dawson, T. R. & Emeson, R. B. Regulation of alternative splicing by RNA editing. *Nature* **399**, 75–80. https://doi.org/10.1038/19992 (1999).
52. Busino, L. et al. SCFFbxl3 controls the oscillation of the circadian clock by directing the degradation of cryptochrome proteins. *Science* **316**, 900–904. https://doi.org/10.1126/science.1141194 (2007).
53. Lamia, K. A. et al. AMPK regulates the circadian clock by cryptochrome phosphorylation and degradation. *Science* **326**, 437–440. https://doi.org/10.1126/science.1172156 (2009).
54. Hirano, A. et al. FBXL21 regulates oscillation of the circadian clock through ubiquitination and stabilization of cryptochromes. *Cell* **152**, 1106–1118. https://doi.org/10.1016/j.cell.2013.01.054 (2013).
55. Brancaccio, M. et al. Astrocytes Control Circadian Timekeeping in the Suprachiasmatic Nucleus via Glutamatergic Signaling. *Neuron* **93**, 1420–1435e5. https://doi.org/10.1016/j.neuron.2017.02.030 (2017).
56. Wen, S. et al. Spatiotemporal single-cell analysis of gene expression in the mouse suprachiasmatic nucleus. *Nat. Neurosci.* **23**, 456–467. https://doi.org/10.1038/s41593-020-0586-x (2020).

57. Golan, N. et al. Identification of Tmem10/Opalin as an oligodendrocyte enriched gene using expression profiling combined with genetic cell ablation. *Glia* **56**, 1176–1186. https://doi.org/10.1002/glia.20688 (2008).
58. He, L. et al. Analysis of the brain mural cell transcriptome. *Sci. Rep.* **6**, 35108. https://doi.org/10.1038/srep35108 (2016).
59. Ben-Zvi, A. et al. Mfsd2a is critical for the formation and function of the blood-brain barrier. *Nature* **509**, 507–511. https://doi.org/10.1038/nature13324 (2014).

Figures

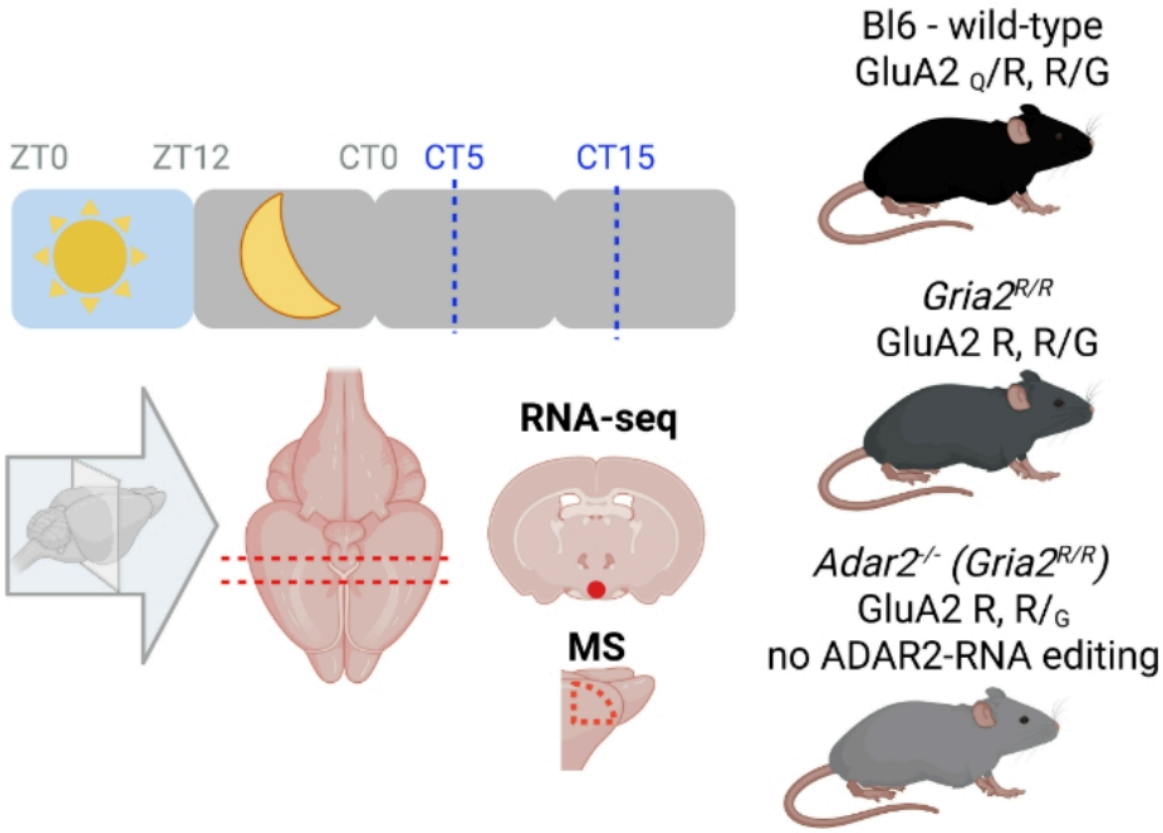


Figure 1

Experimental design for SCN RNA-seq and frontal-cortex proteomic analyses.

Wild-type Bl6, Gria2$^{R/R}$ and Adar2$^{-/-}$ mice were maintained under a LD12:12 and then released into DD to minimize the contribution of acute light-induced transcriptional responses. During the first circadian cycle in

DD, SCN-containing hypothalamic tissue was collected at CT5 and CT15, corresponding to subjective day and subjective night, respectively, and processed for RNA-seq analysis. In parallel, frontal cortex tissue collected at CT15 was processed for mass spectrometry-based proteomic analysis (MS). The scheme also illustrates the genotype and RNA-editing status of the three lines, including wild-type GluA2 Q/R editing in Bl6 mice, constitutive GluA2 R/R expression in Gria2$^{R/R}$ mice and loss of ADAR2-dependent RNA editing in Adar2$^{-/-}$ mice maintained on the Gria2$^{R/R}$ rescue background

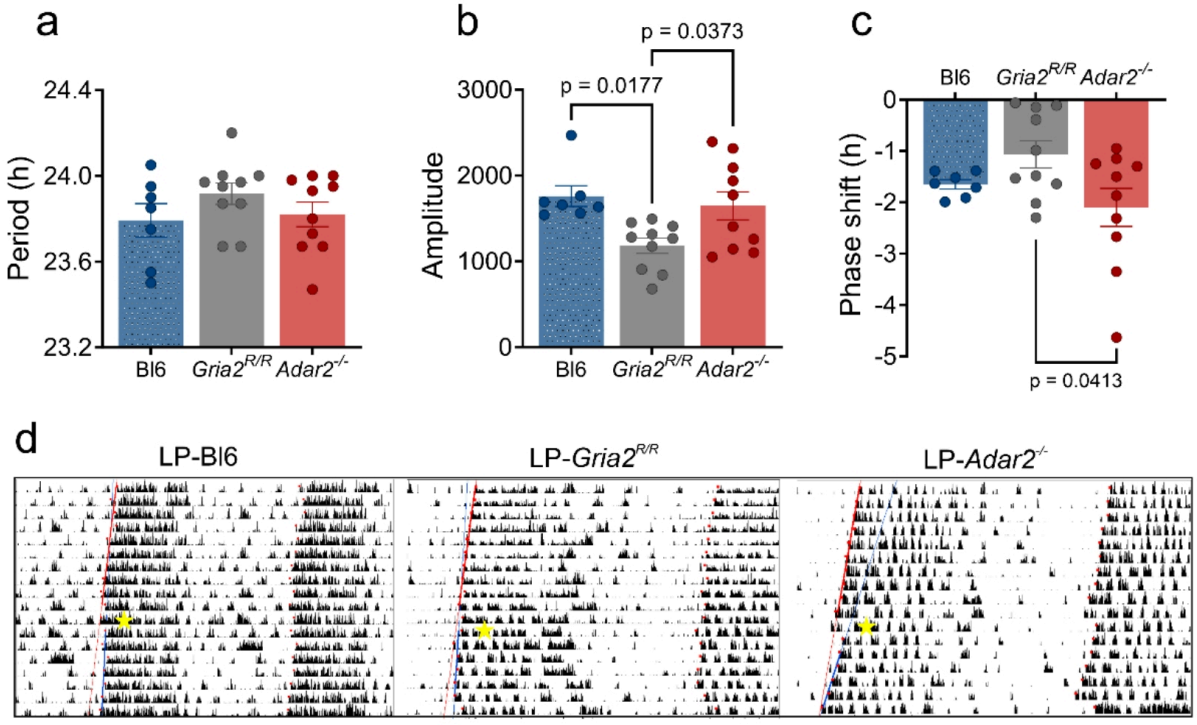


Figure 2

Circadian locomotor rhythms and light-pulse-induced phase shifts in Bl6, Gria2$^{R/R}$ and Adar2$^{-/-}$ mice. *The comparison of circadian period (a), amplitude (b) in locomotor activity rhythm between wild type Bl6, Gria2$^{R/R}$ and Adar2$^{-/-}$ mice and the magnitude of phase delay induced by a 15-min light pulse applied at CT15 (c). The p-values indicate pairwise comparisons from Tukey multiple comparisons test following one-way ANOVA. Data are plotted as mean ± SEM, n = 7-10. (d) Representative actograms in ClockLab format for Bl6, Gria2$^{R/R}$ and Adar2$^{-/-}$ mice. The time of light-pulse (LP) application is indicated by yellow asterisks. Red and blue lines indicate regression lines fitted to activity onsets before and after the light pulse, respectively*

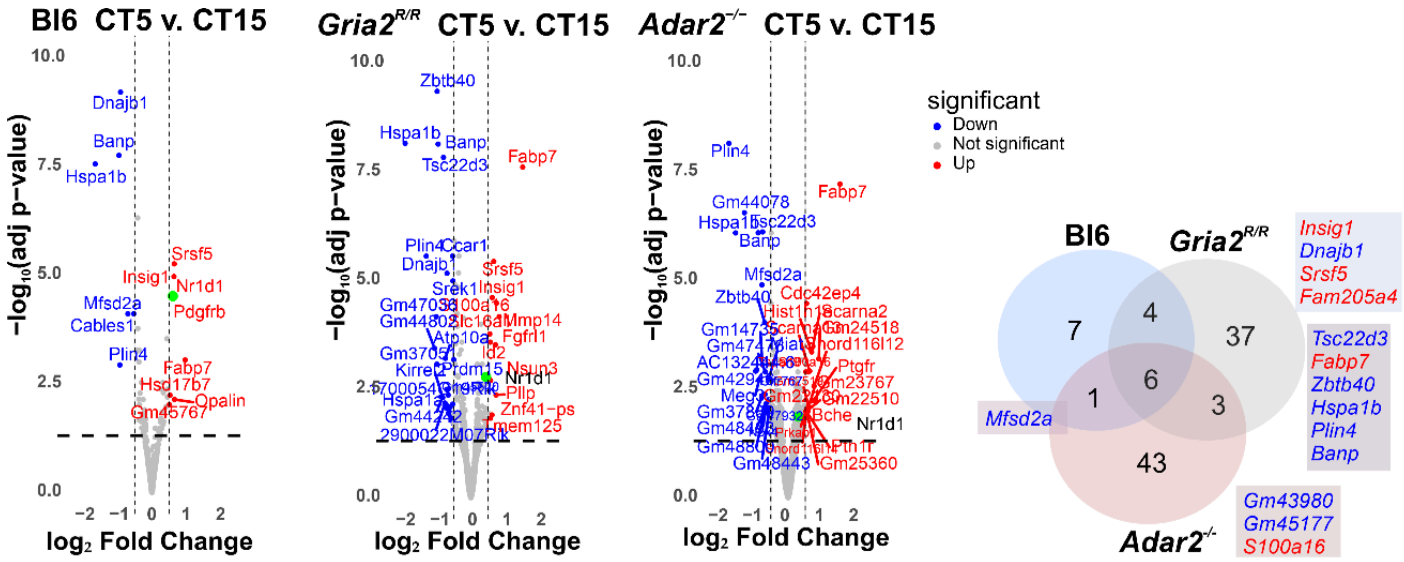


Figure 3

Phase-dependent differential gene expression in the SCN of Bl6, Gria2 $^{R/R}$ and Adar2$^{-/-}$ mice.

Volcano plots show the difference in gene expression at CT5 versus CT15 in the SCN of mice strains. The log_2 fold-change difference on the x-axis is plotted against $-log_{10}$ adjusted p-value on the y-axis. Vertical dashed lines indicate an absolute log_2 fold change of 0.5, corresponding to an approximately 1.4-fold difference, and the horizontal dashed line indicates an adjusted p value of 0.05. Red and blue points indicate genes with higher and lower expression at CT5, respectively, that met both predefined criteria; grey points did not meet both criteria. Green points indicate Nr1d1, highlighted as a canonical clock gene and an internal marker of circadian phase. The Venn diagram shows the overlap between the CT5 and CT15 DEG sets identified in the three genotypes. The adjacent boxes list DEGs shared by all three genotypes or by individual pairs of genotypes

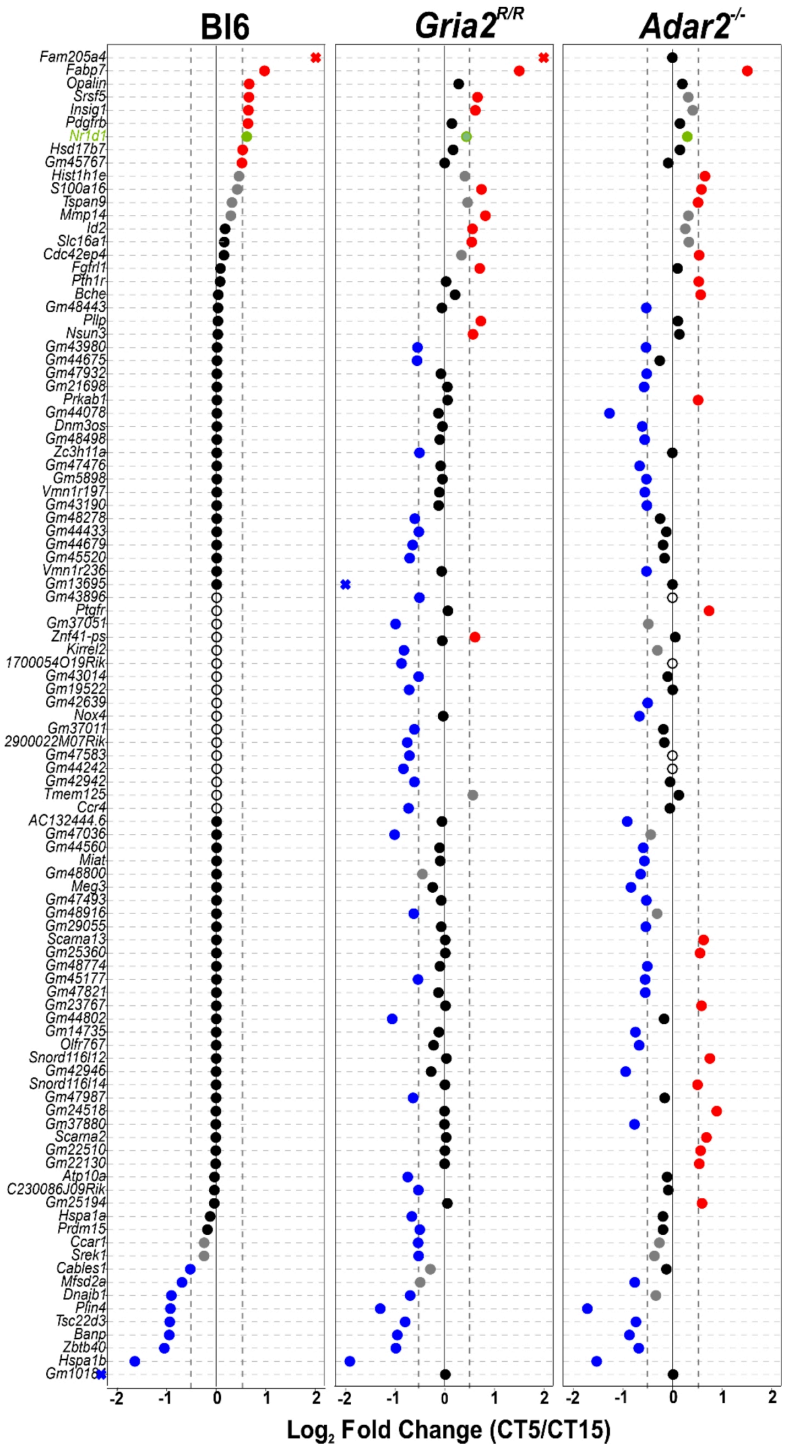


Figure 4

Gene-wise CT5-versus-CT15 fold-change patterns for phase-dependent SCN differentially expressed genes across genotypes. *The plot shows LFC estimates for the 101 genes that met the predefined differential-expression criteria (LFC ≥ 0.5 and adjusted p value ≤ 0.05) in at least one genotype. Each row represents one gene. Genes are ordered according to the CT5-versus-CT15 log2 fold change in Bl6 mice, and the same order is retained in the Gria2$^{R/R}$ and Adar2$^{-/-}$ panels. Positive and negative values indicate*

higher and lower expression at CT5 than at CT15, respectively. Red and blue points indicate genes with positive and negative fold changes, respectively, that met both predefined criteria. Grey points indicate genes with an adjusted p value ≤ 0.05 but an absolute log2 fold change < 0.5. Black points indicate genes with an available adjusted p value > 0.05, whereas open circles indicate genes for which the adjusted p value was unavailable. Green points indicate Nr1d1, highlighted as a canonical clock gene and an internal marker of the CT5-versus-CT15 phase difference. Asterisks at the limits of the x-axis indicate log_2 fold-change estimates outside the displayed range; exact values are provided in Supplementary Table S2

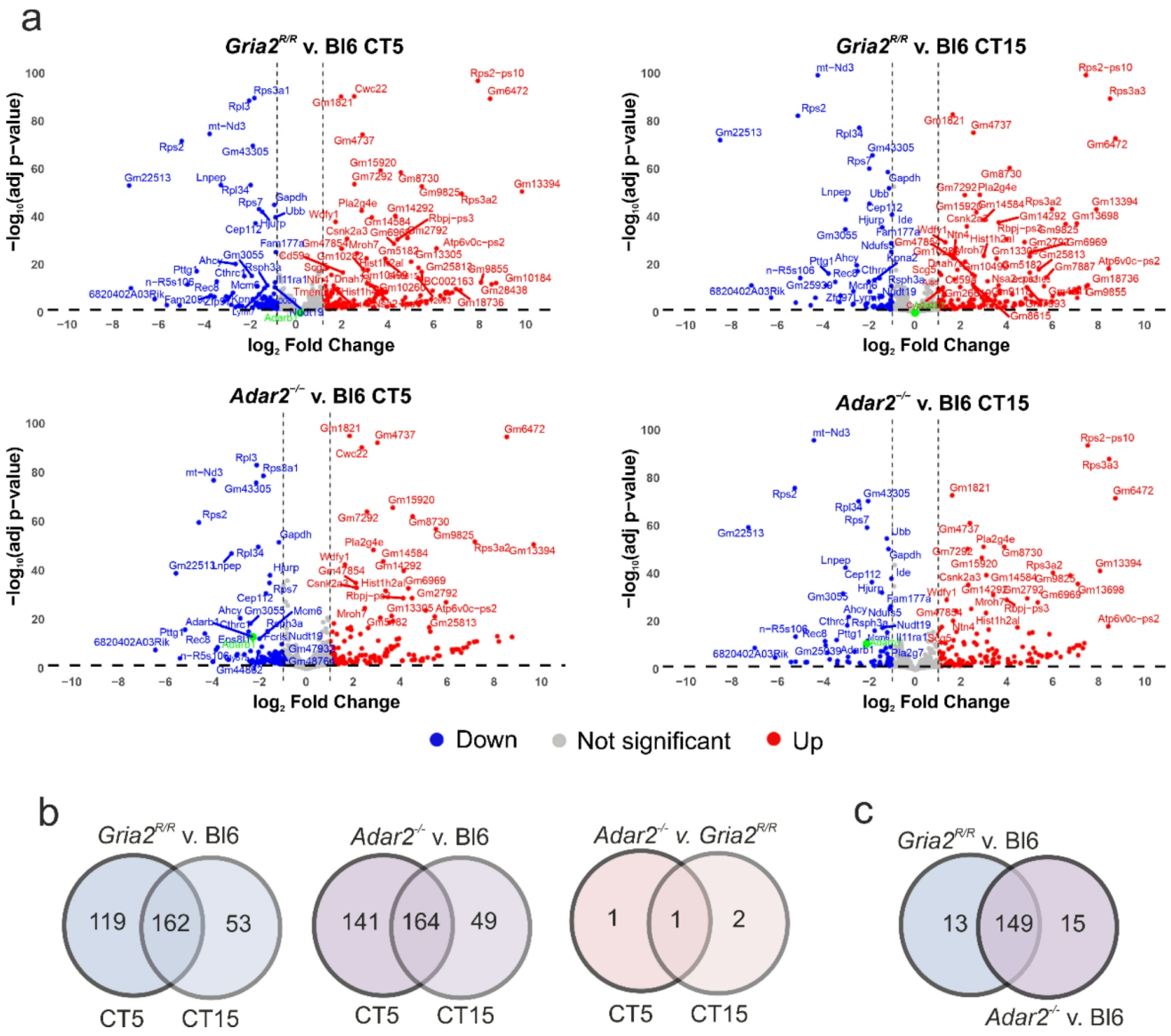


Figure 5

Genotype-dependent differential gene expression in the SCN of Gria2$^{R/R}$ and Adar2$^{-/-}$ mice.

(a) Volcano plots show differential gene expression at CT5 and CT15 in Gria2$^{R/R}$ and Adar2$^{-/-}$ mice relative to Bl6 mice. The x-axis indicates log_2 fold change, with positive and negative values corresponding to higher and lower expression, respectively, in the genetically modified line relative to Bl6. The y-axis indicates $-log_{10}$ adjusted p value. Red and blue points represent genes with higher and lower expression, respectively, that met the predefined differential-expression criteria LFC ≥ 1 and adjusted p value ≤ 0.05). Grey points represent genes that did not meet both criteria. Dashed lines indicate the fold-change and adjusted p-value thresholds. Green points identify Adarb1 irrespective of its differential-expression classification. Adarb1 remained within the non-DEG range in Gria2$^{R/R}$ versus Bl6 comparisons but was significantly downregulated in Adar2$^{-/-}$ mice relative to Bl6 at both CT5 and CT15.

(b) Venn diagrams show the overlap between DEGs identified at CT5 and CT15 for Gria2$^{R/R}$ versus Bl6, Adar2$^{-/-}$ versus Bl6 and Adar2$^{-/-}$ versus Gria2R/R. Numbers indicate genes detected exclusively at CT5, at both time points or exclusively at CT15. Overlap was defined by gene identity irrespective of the direction of expression change.

(c) Venn diagram comparing the combination of DEGs detected at both CT5 and CT15 in the Gria2$^{R/R}$ versus Bl6 and Adar2$^{-/-}$ versus Bl6 contrasts. Of these phase-persistent DEGs, 149 were shared between the two contrasts, whereas 13 and 15 were specific to Gria2$^{R/R}$ and Adar2$^{-/-}$ mice, respectively. Complete gene lists, LFC and adjusted p values are provided in Supplementary Tables 3 and 4

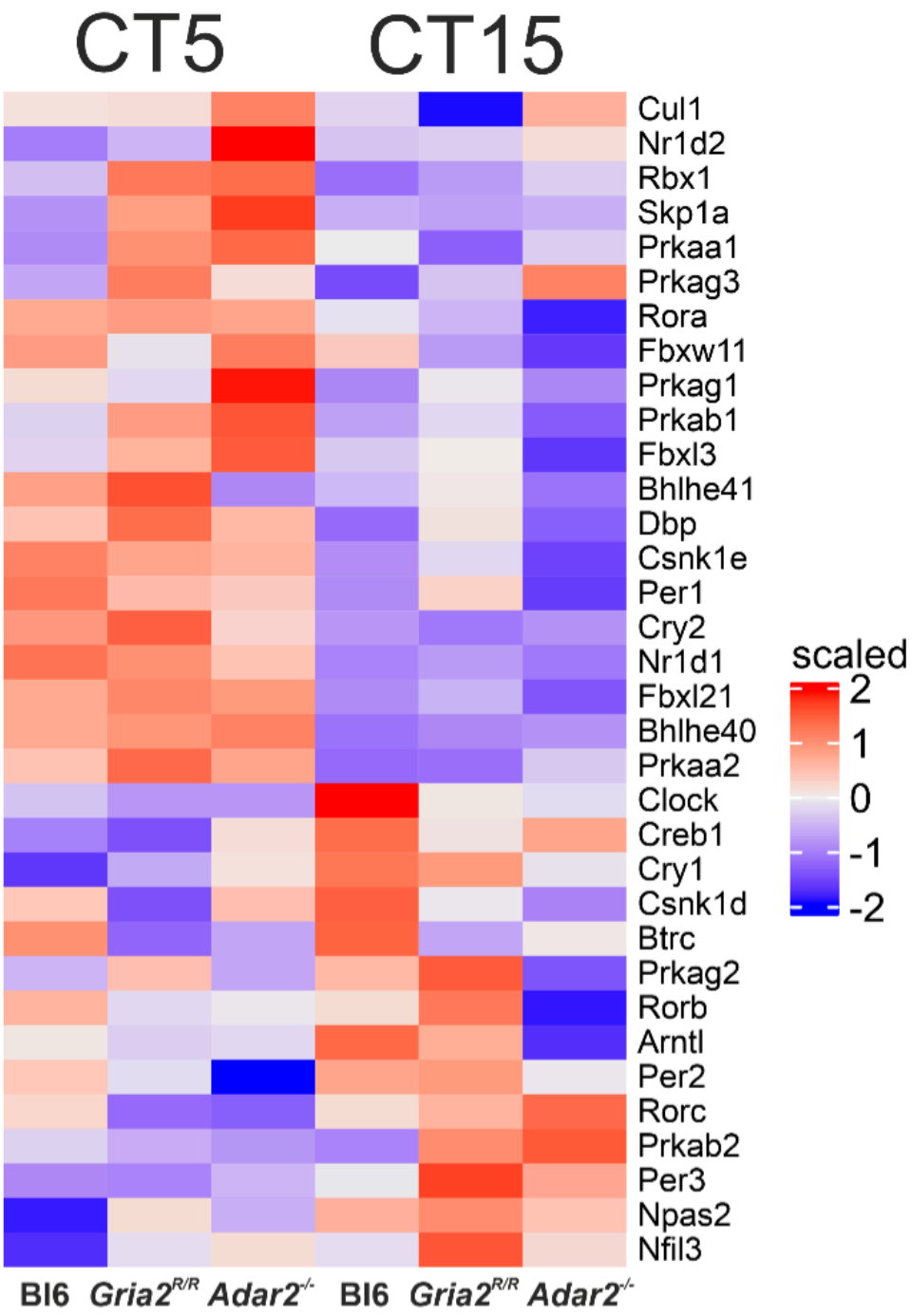


Figure 6

Expression profiles of circadian rhythm pathway genes in the SCN.

The heatmap shows mean rlog-transformed expression values for genes assigned to the KEGG Circadian rhythm pathway (mmu04710) in Bl6, Gria2$^{R/R}$ and Adar2$^{-/-}$ mice at CT5 and CT15. Values were scaled within

each gene to visualise relative expression differences across genotypes and circadian phases. Red indicates higher relative expression and blue indicates lower relative expression

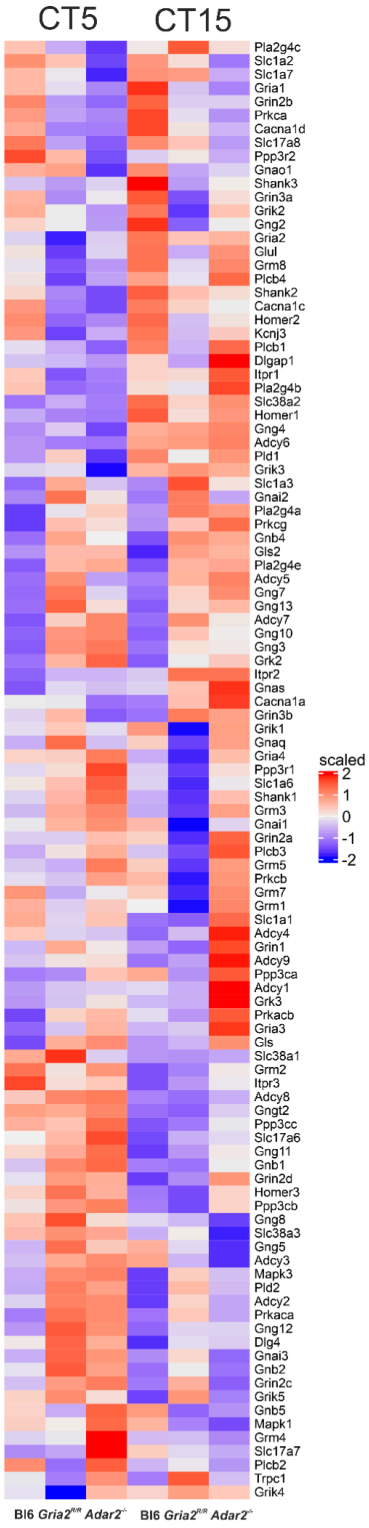


Figure 7

Expression profiles of glutamatergic synapse pathway genes in the SCN.

The heatmap shows mean rlog-transformed expression values for genes assigned to the KEGG Glutamatergic synapse pathway (mmu04724) in Bl6, Gria2$^{R/R}$ and Adar2$^{-/-}$ mice at CT5 and CT15. Values were scaled within each gene to visualise relative expression differences across genotypes and circadian phases. Red indicates higher relative expression and blue indicates lower relative expression

Supplementary Files

This is a list of supplementary files associated with this preprint. Click to download.

- ESM3.xlsx
- ESM2.xlsx
- ESM4.xlsx
- ESM1.pdf
- ESM5.xlsx